

Optical scattering from a planar array of finite-length metallic carbon nanotubes

Jin Hao and George W. Hanson

Department of Electrical Engineering, University of Wisconsin-Milwaukee, Milwaukee, Wisconsin 53211, USA

(Received 8 September 2006; revised manuscript received 25 January 2007; published 25 April 2007)

A model is developed for optical scattering from planar arrays of finite-length single-wall metallic carbon nanotubes. The scattered field is predicted using a periodic Green's function for the array, which includes all electromagnetic interactions, and a quantum conductance function $\sigma_{cn}(\omega)$ for the carbon nanotubes. It is found that for both individual carbon nanotubes and nanotube arrays, the optical far scattered field is proportional to $\sigma_{cn}(\omega)$, so that scattering characteristics are governed by effects associated with electronic transitions. This is in strong distinction to the case for far-infrared arrays, where mutual electromagnetic coupling effects were previously found to be very important for a wide range of broadside nanotube spacings. Furthermore, due to strong damping, single-wall nanotubes do not exhibit longitudinal current resonances (optical antenna effects) associated with the finite length of the tubes, which is also quite different from the far-infrared result.

DOI: [10.1103/PhysRevB.75.165416](https://doi.org/10.1103/PhysRevB.75.165416)

PACS number(s): 78.67.Ch, 73.25.+i, 42.70.-a, 77.84.Lf

I. INTRODUCTION

There is currently considerable interest in the optical properties of nanoscale systems, including the exploration of plasmonic effects for subwavelength optical devices, and the optical response of nanowires and carbon nanotubes (CNs). Possible applications include subwavelength focusing of light, and the development of nanoscale optical antennas. An important aspect of this field is the interaction of an electromagnetic wave with a nanostructure, and here a model is developed for electromagnetic scattering from infinite planar arrays of finite-length single-wall carbon nanotubes (SWNTs), and individual nanotubes, in the optical regime.

The optical behavior of carbon nanotubes has been examined by considering their dielectric function,¹⁻⁶ although in these papers the focus was on the behavior of the dielectric function itself, rather than on optical scattering. A previous model for optical scattering from an isolated CN was presented in Ref. 7 using the Leontovich-Levin integrodifferential equation. Numerical simulations for the scattered electromagnetic field were presented, as well as an iterative analytical solution. In Ref. 8 some antenna properties of individual SWNTs in the optical range have been presented based on the numerical solution of a Hallén's-type integral equation (IE), which was also applied to isolated finite-length nanotubes at GHz and far-infrared frequencies in Ref. 9, and in Ref. 10 to planar arrays in the far-infrared. In Ref. 11 some general aspects of CN antennas at lower frequencies were considered.

Due to the low value of the optical conductance for SWNTs, a simple Born approximation can be used to obtain a closed-form solution for the plane-wave induced current and the far scattered field for isolated nanotubes and nanotube arrays. We show that for nanotubes separated (broadside) by more than a few times the tube's radius, electromagnetic coupling effects are insignificant, and the far scattered field is proportional to $\sigma_{cn}(\omega)$, such that the optical response of an array of nanotubes can be obtained by vectorially summing the contributions of individual nanotubes. This is in strong distinction to the case for far-infrared arrays considered in Ref. 10, where mutual coupling effects (significant

red- and blueshifts in the scattering response, and linewidth broadening) were found to be important, and where the Born approximation was not applicable. Furthermore, due to strong current damping, SWNTs do not exhibit longitudinal current resonances associated with the finite length of the tubes, which is also quite different from the far-infrared case. In the following all units are in the SI system, and the time variation (suppressed) is $e^{j\omega t}$, where j is the imaginary unit.

II. DISCUSSION OF THE MODEL

The geometry of an infinite planar array of finite-length carbon nanotubes is depicted in Fig. 1 (when considering a single isolated tube, only the center element is present). As a practical matter in performing measurements on a finite-sized array having dimensions $L_x \times L_z$, the observation point \mathbf{r} should be far enough from the array plane so that all evanescent waves are negligible, but with $|\mathbf{r}| < L_x, L_z$ so that edge diffraction effects can be ignored.

The electromagnetic model has been developed in Refs. 8-10 based on the fundamental work in Refs. 12-14, and here we briefly summarize the main points. We consider the CN to be a finite-length, infinitesimally thin cylindrical surface of radius a characterized by a local isotropic surface conductance $\sigma_{cn}(S)$ [equivalently, the CN optical dielectric

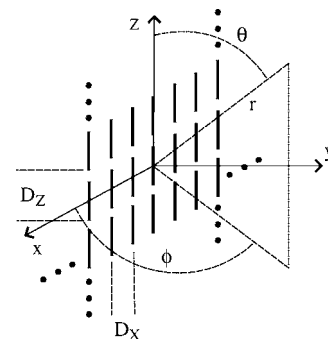


FIG. 1. Infinite planar array of finite-length carbon nanotubes. Each tube has length $2L$, radius a , and the array periods along the x and z axes are D_x and D_z , respectively.

function $\varepsilon_{cn}(\omega)$ could be used]. Assuming that the axis of the CN is the z axis, the electric current density on a CN induced by an external electromagnetic wave is

$$\mathbf{J}(\rho, \phi, z) = \{\hat{\mathbf{z}}J_z(\phi, z) + \hat{\boldsymbol{\phi}}J_\phi(\phi, z)\}\delta(\rho - a). \quad (1)$$

Since we are mainly interested in achiral single-wall tubes, and since $ka \ll 1$ at optical frequencies, where $k = 2\pi/\lambda_0$ is the free-space wave number, we can ignore the azimuthal component of current. This is also a reasonable assumption for chiral tubes, since the geometric chirality factor is much larger than the ratio of azimuthal to longitudinal current¹⁵ (here we are not interested in perpendicular polarization). Since we do not consider arrays with extremely small broadside tube separations we can also ignore the azimuthal variation of the longitudinal current, as well as intertube electronic coupling. With the assumption $\mathbf{J}(\rho, \phi, z) \approx \hat{\mathbf{z}}J_z(z)\delta(\rho - a)$, the exact solution of Maxwells equations for the CN geometry depicted in Fig. 1 is given by the solution of the Pocklington equation,

$$\frac{I(z)}{2\pi a \sigma_{cn}} = \frac{1}{j4\pi\omega\epsilon} \left(k^2 + \frac{\partial^2}{\partial z^2} \right) \int_{-L}^L K(z - z') I(z') dz' + E_z^i(z), \quad z \in (-L, L), \quad (2)$$

where $I(z) = J_z(z)2\pi a$, ω is the radian frequency, ϵ is the permittivity of the material surrounding the tubes (here assumed to be free space), and E_z^i is the z component of the incident electric field. The Pocklington equation is valid for both an individual nanotube and for an infinite array of nanotubes, where in the former case the kernel function $K(z - z')$ is related to the usual scalar free-space Green's function, and in the latter case $I(z)$ is the current on the center tube of the array, and the kernel is related to the periodic Green's function. By applying Floquet's theorem¹⁶ all of the current distributions on the other array elements are obtained by phase shifting from the center tube. The details for both cases are provided in Ref. 10.

An important aspect of the model is the quantum conductance $\sigma_{cn}(\omega)$. For numerical calculations we use a π -electron tight-binding result,¹²⁻¹⁴ which includes interband transitions but not curvature and many-body effects. Curvature effects are particularly important in very small radius tubes,² and, given the quasi-one-dimensional nature of SWNTs, excitonic effects are also expected to be quite important in many situations, especially for semiconducting tubes.^{17,18} These effects can be included, e.g., by using *ab initio* calculations;^{2,18,19} as a concrete example, the optical complex dielectric function $\varepsilon_{cn}(\omega)$ for (3,3), (5,0), and (4,2) nanotubes are given in Ref. 2, from which the conductance can be determined as $\sigma_{cn} = j\omega\epsilon_0[\varepsilon_{cn}(\omega) - 1]/S\rho_T$, where S is the surface area of the nanotube and ρ_T is the volume density of tubes.¹² However, a principle contribution of this work is to develop the analytical CN array far-field scattering solution based on the Born approximation, the validity of which is independent of the method used to obtain $\sigma_{cn}(\omega)$ and only requires that the optical conductance be sufficiently small, as explained below.

A. Born approximation

In Ref. 10, Pocklington's equation (2) for an infinite planar array of carbon nanotubes was solved by converting it to a Hallén's-type integral equation and using a method-of-moments pulse function expansion, point matching numerical procedure. However, in that work the formulation was applied in the far-infrared, where the carbon nanotube conductance is relatively large, $|\sigma_{cn}| \sim 10^{-2}$ (S). However, in the optical range σ_{cn} is several orders of magnitude smaller. For example, for the single-wall metallic tubes considered in Refs. 12 and 20, $|\sigma_{cn}| \sim 10^{-4} - 10^{-5}$ (i.e., on the order of e^2/h) through most of the optical range, peaking to approximately 10^{-3} at interband transition frequencies. These values are consistent with the *ab initio* dielectric function calculations in Ref. 2. Because of this low conductance, the expression on the left side of Eq. (2) is much larger than the first term on the right side, which, to a first-order approximation, can be ignored. This is essentially the Born approximation (BA),^{21,22} where the small σ_{cn} plays the role of a small material contrast. Thus the Born approximation for the nanotube current, in both the individual tube and planar array cases, is simply

$$I_{BA}(z, \omega) = 2\pi a \sigma_{cn}(\omega) E_z^i(z). \quad (3)$$

Although it may seem that the nanoscale radius a also plays a role in the dominance of the left side of Eq. (2), it can be shown that for an isolated tube the kernel function can be written as²³

$$K(z - z') = -\frac{1}{\pi a} \ln|z - z'| + K_1(z - z'), \quad (4)$$

where K_1 is a continuous function with a bounded derivative. Therefore the radius a occurs in the dominate singularity of the kernel as well, and it is therefore the small conductance that controls the size of the left side term in Eq. (2). Importantly, the same can be shown for the periodic (infinite array) kernel.

The question of how small the nanotube conductance should be for the Born approximation to be accurate is difficult to answer precisely, due to the complicated nature of the Pocklington kernel. However, dimensional analysis²² shows that the Born approximation should be valid when

$$\Delta_{BA} = \frac{|\sigma_{cn}|}{\omega\epsilon_0} (k^2 + L^{-2})L \ll 1. \quad (5)$$

Predictions using Eq. (5) corollate with numerical tests comparing the Born approximation and the integral equation result (see Table I) and indicate that the BA is applicable in the near-infrared and optical regimes, where $|\sigma_{cn}| \sim 10^{-4} - 10^{-5}$ (S). Although a comprehensive study across different nanotubes was not made, this was found to be true for a wide range of armchair and zigzag nanotubes. Of course, some error is expected in Eq. (3) near the nanotube ends, where the actual current vanishes but the incident field obviously does not. However, given that one is typically interested in tubes such that $L/a \gg 1$, the Born approximation will provide a suitable result over most of the length of the nanotube. For an isolated carbon nanotube a comprehensive approximate

TABLE I. Relative error arising from the Born approximation for an isolated nanotube. The third and fourth columns are the relative error percentages between the current at the center of the nanotube ($z=0$) and at one-quarter of the tube length from the tube ends ($z=0\pm L/2$), computed by the integral equation and the Born approximation. The fourth column is the L_2 error between the two solutions. $L=100$ nm, $a=1$ nm, and $f=500$ THz (2.068 eV).

σ_{cn} (S)	Δ_{BA}	% Rel. error $I(0)$	% Rel. error $I(0\pm L/2)$	L_2 error
10^{-6}	0.000754	0.0015	0.000855	0.0104
10^{-5}	0.00754	0.0149	0.00855	0.0330
10^{-4}	0.0754	0.1486	0.0824	0.1168
10^{-3}	0.754	1.4915	2.2749	0.6226
10^{-2}	7.54	14.25	25.50	3.5905
10^{-1}	75.4	128.9	181.3	32.53

analytical solution, based on an iterative approach involving the propagation constant of an infinite-length nanotube, is presented in Ref. 7.

Table I shows the relative error in the current arising from the Born approximation for an isolated nanotube. As an example of a typical carbon nanotube, we take $L=100$ nm, $a=1$ nm, $f=500$ THz (2.068 eV), and $|E_z^i|=1$, and vary σ_{cn} . The third and fourth columns are the relative error percentages between the current at the center of the nanotube ($z=0$) and at one-quarter of the tube length from the tube ends ($z=0\pm L/2$), computed by the integral equation and the Born approximation (3). The last column is the L_2 relative error between the two solutions. It can be seen that the estimate Δ_{BA} can be used to gauge the suitability of the Born approximation. For $\sigma_{cn} < 10^{-3}$, the relative error is fairly low, and therefore the Born approximation is applicable in the near-infrared and optical regime. In the far-infrared $\sigma_{cn} \sim 10^{-2}$ (S) or larger,¹² and assuming typical parameters (5) indicates that the Born approximation is not valid.

The Born approximation for the current is considered in Fig. 2, where the magnitude of the current at the center (z

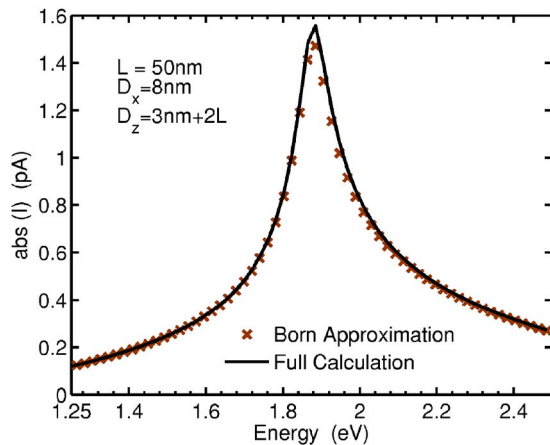


FIG. 2. (Color online) Magnitude of the current at the center ($z=0$) of the center nanotube in an infinite array of (10, 10) nanotubes, calculated from the Born approximation (3) and from the numerical solution of the integral equation for the array case.

$=0$) of the center nanotube in the array is shown as a function of energy, calculated from the Born approximation (3) and from the numerical solution of the integral equation for the array case (the numerical parameters used to calculate σ_{cn} will be discussed Sec. II B). The agreement is excellent, verifying the Born approximation at least for the considered geometry (the same level of agreement was obtained for other nanotubes considered). Therefore the electromagnetic mutual coupling effects that are accounted for by the infinite array kernel $K(z-z')$, which are neglected in the Born approximation, are clearly of minor importance. In effect, although the tubes are metallic in nature (i.e., they do not have a band gap), in the optical regime they lead to weak perturbations of the background environment.

After the currents are determined the far scattered electric field can be found. Details are provided in Ref. 10, although for optical frequencies (3) can be used to obtain a closed-form solution for both individual nanotubes and nanotube arrays. For an individual nanotube oriented along the z axis, the far scattered field can be written as $\mathbf{E}^s = \hat{\theta} E_\theta^s(r, \theta)$, and under the Born approximation (a factor of $\sin \theta$ was missing from Ref. 10 [Eq. (8)])

$$E_{\theta,BA}^s(r, \theta, \omega) = 2\pi a \sigma_{cn}(\omega) j \omega \mu_0 \frac{e^{-jkr}}{4\pi r} \times \sin \theta \int_{-L}^L E_z^i(z') e^{jkz' \cos \theta} dz'. \quad (6)$$

Assuming an incident plane wave, then along the axis of the nanotube $E_z^i(z) = E_0 e^{jkz \cos \theta'}$, where $0 < \theta' < 180^\circ$ is the angle of the incident wave vector measured from the z axis. In this case

$$E_{\theta,BA}^s(r, \theta, \omega) = 2\pi a \sigma_{cn}(\omega) j \omega \mu_0 E_0 \frac{e^{-jkr}}{4\pi r} \times \sin \theta \frac{2 \sin[kL(\cos \theta' + \cos \theta)]}{k(\cos \theta' + \cos \theta)}, \quad (7)$$

and, in particular, for $\theta' = \theta = 90^\circ$

$$\left| \frac{E_{\theta,BA}^s(r, \omega)}{E_0} \right| = \frac{a \omega \mu_0 L |\sigma_{cn}(\omega)|}{r}. \quad (8)$$

For an infinite array the BA scattered field $\mathbf{E}_{BA}^s(\omega)$ is obtained by substituting Eq. (3) in Ref. 10 [Eqs. (9)–(11)] and integrating over the Born-approximated current. A further approximation leading to a simple result is to note that, since D_x^{-1} and D_z^{-1} are on the order of 10^9 m⁻¹, and in the optical range the wave number k is on the order of 10^6 – 10^7 m⁻¹, only the zeroth-index term in the summation in Ref. 10 [Eq. (9)] leads to propagating plane waves. For example, for a plane-wave incidence angle of $\theta' = 90^\circ$ and $0 < \theta' < 180^\circ$, and an observation angle of $\theta = 90^\circ$ and $0 < \theta < 180^\circ$, the magnitude of the zeroth-order array Born approximation (ZO array BA) is

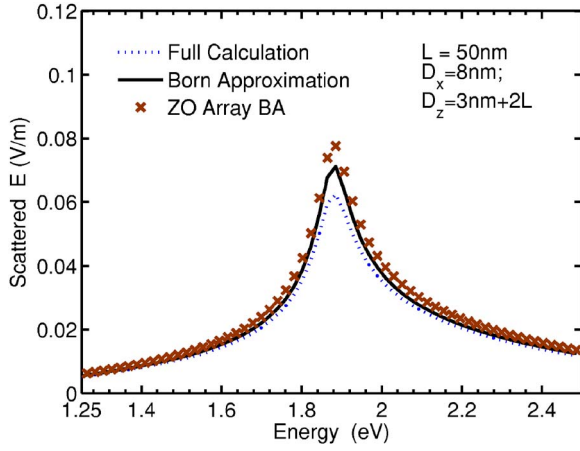


FIG. 3. (Color online) Comparison between the IE solution and the Born approximations \mathbf{E}_{BA}^s and $\mathbf{E}_{BA,0}^s$ for the far scattered field from an infinite planar array of (10, 10) carbon nanotubes. The field is incident from $\theta^i=90^\circ$ and $\phi^i=30^\circ$, and the scattered field is determined at $\theta=90^\circ$ and $\phi=150^\circ$ (i.e., specular reflection), at a distance of $r=1 \mu\text{m}$.

$$\begin{aligned} \left| \frac{\mathbf{E}_{BA,0}^s(\omega)}{E_0} \right| &= \frac{2\pi a L \eta_c |\sigma_{cn}(\omega)|}{D_x D_z} \sqrt{\cos^2 \phi^i + \frac{1}{\sin^2 \phi^i}} \\ &\simeq \left| \frac{\mathbf{E}_{BA}^s(\omega)}{E_0} \right|, \end{aligned} \quad (9)$$

where $\eta_c = \sqrt{\mu_0/\epsilon_0} \approx 377 \Omega$. From both Eqs. (7) and (9) we conclude that the far scattered field from a carbon nanotube and nanotube array is proportional to $\sigma_{cn}(\omega)$.

The nanotube length dependence can be removed from the scattered field expression (9) for many arrays of interest, where the longitudinal gap between adjacent nanotube ends is small compared to the tube length. Denoting the longitudinal gap spacing between adjacent tubes as δ_z , and noting that D_z is the center-to-center longitudinal separation between nanotubes, then $D_z = \delta_z + 2L$. Assuming that $2L \gg \delta_z$, Eq. (9) simplifies to the length-independent zeroth-order scattered field,

$$\left| \frac{\mathbf{E}_{BA,0}^s(\omega)}{E_0} \right| \simeq \frac{\pi a \eta_c |\sigma_{cn}(\omega)|}{D_x} \sqrt{\cos^2 \phi^i + \frac{1}{\sin^2 \phi^i}}. \quad (10)$$

The ratio of the zeroth-order scattered field from an array and the scattered field from an individual nanotube is

$$R_s = \frac{2\pi r}{D_x D_z k} \sqrt{\cos^2 \phi^i + \frac{1}{\sin^2 \phi^i}}. \quad (11)$$

Given that in the optical range $k \sim 10^7 \text{ m}^{-1}$, and choosing, for example, $D_x = 10 \text{ nm}$, $D_z = 100 \text{ nm}$, $r = 1 \mu\text{m}$, and $\phi^i = 30^\circ$, then $R_s = 1382r$, where r is in microns. Thus for measurement distances on the order of microns, the scattered field from an infinite planar array will be several orders of magnitude larger than the scattered field from an individual nanotube.

Figure 3 shows a comparison between the IE solution and the Born approximations \mathbf{E}_{BA}^s and $\mathbf{E}_{BA,0}^s$ for the far scattered field of an infinite planar array. It can be seen that the BA and

the simple zeroth-order array BA overestimate the peak values by approximately 11% and 21%, respectively.

B. Model verification and results

1. Comparison with measurement

For the numerical results presented here we use the tight-binding conductance developed in Ref. 12–14. There are two parameters to choose; $\nu = \tau^{-1}$, the phenomenological relaxation frequency, and γ_0 , the overlap integral. The location of van Hove singularities for metallic tubes is given by²⁴ $E_s = 3sb\gamma_0/2a$, $s=1,2,3,\dots$, and the energy of dipole-allowed transitions between van Hove singularities is $2E_s$, so that γ_0 plays an important role in predicting the location of scattering or absorbance peaks. Reported values of γ_0 cover the range 2.5–3.1 eV, with values at the lower end of the range associated with low-frequency measurements,^{25,26} and those at the upper end of the range associated with optical experiments.^{27,28} Here we use $\gamma_0 = 3.03 \text{ eV}$ which is associated with two-dimensional graphite (Ref. 29, p. 32), and agrees with the CN optical value reported in Ref. 28.

The second model parameter to choose is the relaxation frequency $\nu = \tau^{-1}$. Interactions with optical phonons, which may be expected to dominate relaxation, lead to fairly short relaxation times, and these will depend on energy and tube chirality. For moderate radius nanotubes such as the (10, 10) tube, a theoretical estimate for electron-optical phonon interactions is $\tau = 0.08 \text{ ps}$,³⁰ and experimental values are $\tau = 0.01 \text{ ps}$,³¹ and $\tau = 0.016 \text{ ps}$.³² Photoemission measurements for similar radius tubes lead to $\tau = 0.015 \text{ ps}$ at 2 eV.³³ In the following numerical results we consider (10, 10) tubes and use $\tau = 0.01 \text{ ps}$, which leads to very good agreement with Rayleigh scattering measurements.³⁴

In subsequent numerical results the incident field is a unit-amplitude uniform plane wave, incident on the nanotube(s) at angles $\theta^i = 90^\circ$ and $\phi^i = 30^\circ$. The scattered field is then determined at observation angles $\theta = 90^\circ$ and $\phi = 150^\circ$ (i.e., specular reflection), at a distance of $r = 1 \mu\text{m}$. For the array case, this is far enough from the array to attenuate all evanescent waves to yield a distance-independent scattered field¹⁰ (for an isolated nanotube the scattered field will retain a distance-dependent factor r^{-1}). In the following results the scattered electric field is $E = |\mathbf{E}^s| \simeq |E_\theta^s|$, and the numerical solution of the integral equation is shown unless otherwise specified.

In Ref. 10 very good agreement was shown between the integral equation solution and a Rayleigh scattering measurement for a (10, 10) nanotube.³⁴ This result is repeated as Fig. 4, where we have added results for the array case and the Born approximation (9). Since absolute amplitudes are not available from the measurement, all curves have been normalized to unity.

Comparing the array and isolated tube results, it can be seen that the scattering peak location and line shape are essentially independent of electromagnetic coupling between the nanotubes. This is in agreement with the Born approximations (8) and (9), where only an amplitude term linear in frequency distinguishes the far fields from an individual tube and from an infinite array of tubes.

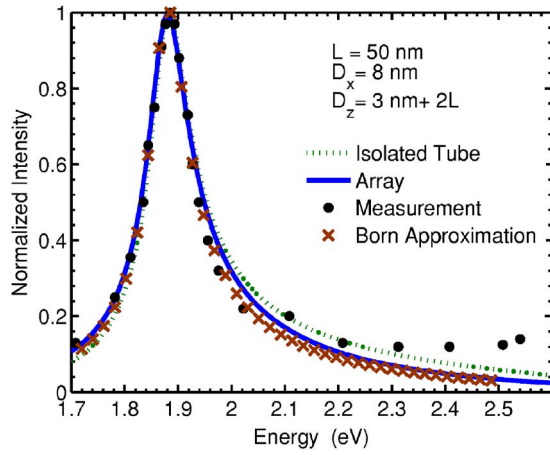


FIG. 4. (Color online) Normalized scattered field intensity of an isolated (10, 10) carbon nanotube from simulation and measurement, and for an infinite array of nanotubes. The peak electric-field values for the isolated tube and for the infinite array of tubes are 4.153×10^{-5} and 0.0626 V/m, respectively. The Born approximation (9) for the infinite array is also shown.

In Fig. 5 a comparison is shown between the integral equation solution and a Rayleigh scattering measurement³⁴ for an isolated (11, 8) chiral metallic carbon nanotube. For the simulation we used a tight-binding dielectric function $\epsilon_{cn}(\omega)$ modified from Ref. 1 to approximately hold in the chiral case. Conductance is then obtained as $\sigma_{cn} = j\omega\epsilon_0[\epsilon_{cn}(\omega) - 1](2a + d)^2/2\pi a$, where $d = 0.34$ nm is the intertube distance in a square lattice of tubes [in Ref. 1 intertube interaction was ignored, so that $\epsilon_{cn}(\omega)$ is governed by a single tube]. The agreement between measurement and simulation is fair, although obviously less satisfactory than in the preceding case. However, the physics of this configuration is much more complicated since there is a splitting of electronic transitions in the metallic chiral case due to the trigonal warping effect associated with band distortions.^{28,35} This is clearly shown in the simulation result, although the agreement with measurement is rather qualitative. Since the far

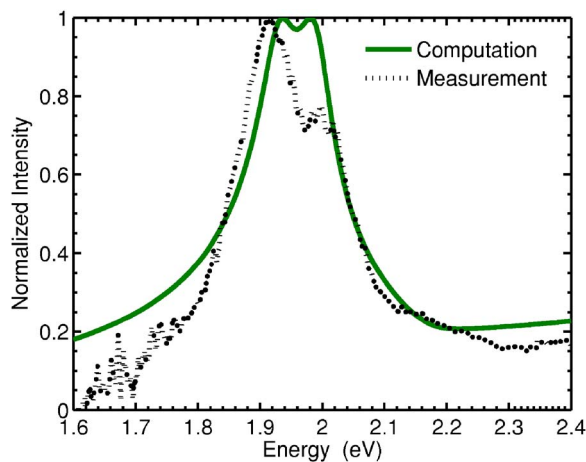


FIG. 5. (Color online) Normalized scattered field intensity of an isolated (11, 8) carbon nanotube from simulation (with $\tau = 2.2$ fs) and measurement.

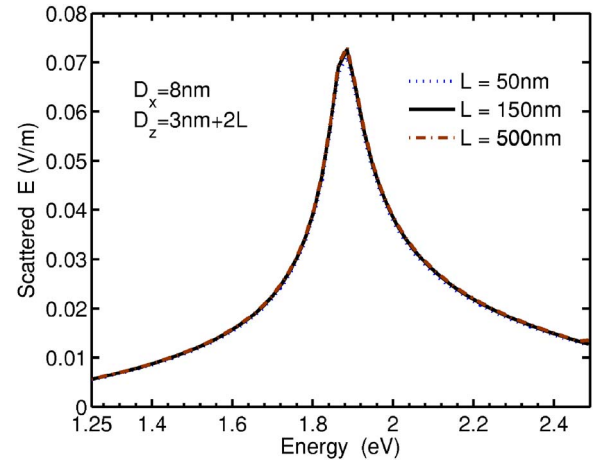


FIG. 6. (Color online) Scattered electric field from an array of (10, 10) carbon nanotubes ($D_x = 8$ nm and $D_z = 3$ nm + $2L$). The nanotubes have half lengths $L = 50, 150,$ and 500 nm.

scattered field is proportional to $\sigma_{cn}(\omega)$, excellent agreement would be expected when using an *ab initio* dielectric function. Indeed, the use of a nonorthogonal tight-binding dielectric function⁵ shows two unequal scattering peaks, with a peak-to-peak spacing that corresponds to the measurement (although the higher-energy peak is larger). However, this result is not shown in Fig. 5 since $\epsilon_{cn}(\omega)$ did not include any broadening, and so the linewidth is very small.

2. Mutual coupling effects in optical arrays—Nanotube length dependence and broadside spacing effects

As discussed in Refs. 7 and 8, in the near-infrared and optical regimes $\sigma_{cn}(\omega)$ is very small, and current is strongly damped on the tubes. Therefore nanotube length-dependent longitudinal current resonances do not seem to occur, and the scattering characteristics are dominated by effects associated with electronic transitions. This is shown in Fig. 6, where the scattered fields are essentially identical for three different

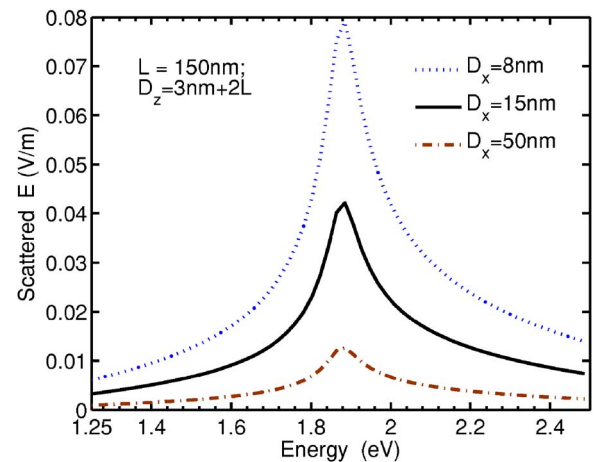


FIG. 7. (Color online) The scattered electric field from several different array configurations of (10, 10), $L = 150$ -nm carbon nanotubes. In all cases the end-to-end spacing ($\delta_z = D_z - 2L$) is 3 nm, and the broadside spacing D_x is varied.

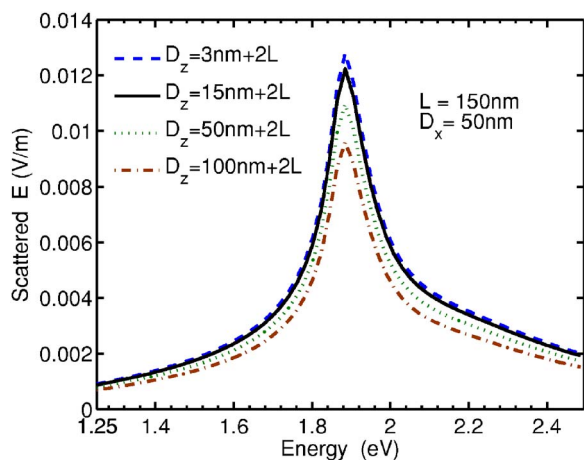


FIG. 8. (Color online) The scattered electric field from several arrays of (10, 10) carbon nanotubes. In all cases $L=150$ nm and $D_x=50$ nm, and D_z is varied.

length carbon nanotubes in an array configuration. This is in agreement with the Born prediction (10).

Figure 7 shows broadside coupling effects (side-to-side spacing D_x is varied) on the scattered field for an array consisting of $L=150$ -nm carbon nanotubes. It can be seen that the only difference is in the scattered amplitude, as predicted by the Born approximation (9), since smaller values of D_x lead to more tubes per unit area.

3. Mutual coupling effects in optical arrays—End-to-end spacing

Figure 8 shows the effect of end-to-end spacing on the scattering characteristics for carbon nanotube arrays consisting of $L=150$ -nm nanotubes. As would be expected from physical considerations and the Born results (9) and (10), the longitudinal end-to-end nanotube spacing only affects the scattered amplitude, and relatively less variation is seen compared to the effect of broadside spacing, unless the gap spacing becomes similar to the tube length.

4. Optical antenna effects

Finally, some comments on the interesting optical antenna effect reported in Refs. 36 and 37 are in order. In those studies relatively large-radius, multiwall nanotubes were measured. For example, the radius of the multiwall nanotube in Ref. 36 was $a=25$ nm. By assuming the multiwall tube to

be equivalent to a large radius single-wall tube, a numerical study based on integral equation (2) shows that simply increasing the tube radius to be 25 nm while maintaining the optical conductance to be a typical value, $\sigma_{cn} \sim 10^{-5}$ (S), does not lead to optical antenna effects, since the current is still highly damped along the tube. However, if $a=25$ nm and $\sigma_{cn} \sim 10^{-3}$ (S) or larger, current resonances can begin to form, leading to the classic antenna effect (e.g., resonant response at odd integer multiples of a half wavelength). As a rough approximation, a large-radius, relatively thin-walled multiwall tube can be modeled as a single-wall tube with an effective radius $a^{eff}=(a_1+a_2)/2$ and effective conductance $\sigma_{cn}^{eff}=N\sigma_{cn}$, where a_1 is the radius of the inner wall, a_2 is the radius of the outer wall, and N is the number of concentric tubes.¹² Assuming a^{eff} is 25 nm implies that one must have on the order of 100 concentric tubes to observe the antenna effect. Although this model ignores intertube interactions, and so provides only a rough guide, it seems likely that the observed antenna effect in multiwall tubes is primarily the result of a larger effective surface conductance, and to a lesser degree to a larger effective radius. However, this warrants further study.

III. CONCLUSIONS

Electromagnetic scattering from finite-length single-wall metallic carbon nanotubes, both isolated and in an infinite planar array configuration, have been investigated using an integral equation technique in the optical regime. A simple Born approximation has been shown to be applicable, leading to a closed-form approximation for the nanotube current and far-scattered field, both of which are proportional to $\sigma_{cn}(\omega)$. The Born results predict that the scattered far field is governed by effects associated with electronic transitions, and that array spacing and tube length primarily affect the scattered field amplitude.

ACKNOWLEDGMENTS

The authors would like to thank Matt Sfeir, Brookhaven National Laboratory, for providing the (10,10) and (11,8) Rayleigh measurement data and dielectric function code in the chiral case, and for helpful discussions. The authors would also like to thank Valentin Popov, University of Sofia, Bulgaria for supplying the (11,8) nonorthogonal tight-binding dielectric function data.

¹M. F. Lin and Kenneth W.-K. Shung, Phys. Rev. B **50**, 17744 (1994).

²M. Machón, S. Reich, C. Thomsen, D. Sánchez-Portal, and P. Ordejón, Phys. Rev. B **66**, 155410 (2002).

³C. D. Spataru, S. Ismail-Beigi, L. X. Benedict, and S. G. Louie, Phys. Rev. Lett. **92**, 077402 (2004).

⁴M. Y. Sfeir, F. Wang, L. Huang, C.-C. Chuang, J. Hone, S. P. O'Brien, T. F. Heinz, and L. E. Brus, Science **306**, 1540 (2004).

⁵V. N. Popov and L. Henrard, Phys. Rev. B **70**, 115407 (2004).

⁶V. N. Popov and P. Lambin, Phys. Rev. B **74**, 075415 (2006).

⁷G. Ya. Slepyan, M. V. Shuba, S. A. Maksimenko, and A. Lakhatakia, Phys. Rev. B **73**, 195416 (2006).

⁸J. Hao and G. W. Hanson, IEEE Trans. Nanotechnol. **5**, 766 (2006).

⁹G. W. Hanson, IEEE Trans. Antennas Propag. **53**, 3426 (2005).

¹⁰J. Hao and G. W. Hanson, Phys. Rev. B **74**, 035119 (2006).

- ¹¹P. J. Burke, S. Li, and Z. Yu, *IEEE Trans. Nanotechnol.* **5**, 314 (2006).
- ¹²G. Y. Slepyan, S. A. Maksimenko, A. Lakhtakia, O. Yevtushenko, and A. V. Gusakov, *Phys. Rev. B* **60**, 17136 (1999).
- ¹³S. A. Maksimenko and G. Y. Slepyan, in *Electromagnetic Fields in Unconventional Materials and Structures*, edited by O. N. Singh and A. Lakhtakia (Wiley, New York, 2000).
- ¹⁴S. A. Maksimenko and G. Y. Slepyan, in *The Handbook of Nanotechnology-Nanometer Structures/Theory, Modeling, and Simulation*, edited by A. Lakhtakia (SPIE Press, Bellingham, WA, 2004).
- ¹⁵Y. Miyamoto, S. G. Louie, and M. L. Cohen, *Phys. Rev. Lett.* **76**, 2121 (1996).
- ¹⁶L. Brillouin, *Wave Propagation in Periodic Structures* (Dover, New York, 1953).
- ¹⁷F. Wang, G. Dukovic, L. E. Brus, and T. F. Heinz, *Science* **308**, 838 (2005).
- ¹⁸V. Barone, J. E. Peralta, and G. E. Scuseria, *Nano Lett.* **5**, 1830 (2005).
- ¹⁹E. Chang, G. Bussi, A. Ruini, and E. Molinari, *Phys. Rev. B* **72**, 195423 (2005).
- ²⁰S. Tasaki, K. Maekawa, and T. Yamabe, *Phys. Rev. B* **57**, 9301 (1998).
- ²¹J. D. Jackson, *Classical Electromagnetics*, second edition (John Wiley, New York, 1975).
- ²²W. C. Chew, *Waves and Fields in Inhomogeneous Media* (IEEE Press, Piscataway, NJ, 1995).
- ²³D. S. Jones, *IEE Proc., Part H: Microwaves, Opt. Antennas* **128**, 114 (1981).
- ²⁴J. W. Mintmire and C. T. White, *Phys. Rev. Lett.* **81**, 2506 (1998).
- ²⁵J. W. G. Wildöer, L. C. Venema, A. G. Rinzler, R. E. Smalley, and C. Dekker, *Nature (London)* **391**, 59 (1998).
- ²⁶T. W. Odom, J.-L. Huang, P. Kim, and C. M. Lieber, *Nature (London)* **391**, 62 (1998).
- ²⁷A. Hagen and T. Hertel, *Nano Lett.* **3**, 383 (2003).
- ²⁸R. Saito, G. Dresselhaus, and M. S. Dresselhaus, *Phys. Rev. B* **61**, 2981 (2000).
- ²⁹R. Saito, G. Dresselhaus, and M. S. Dresselhaus, *Physical Properties of Carbon Nanotubes* (Imperial College Press, London, 2003).
- ³⁰J. Jiang, R. Saito, Ge. G. Samsonidze, S. G. Chou, A. Jorio, G. Dresselhaus, and M. S. Dresselhaus, *Phys. Rev. B* **72**, 235408 (2005).
- ³¹J.-Y. Park, S. Rosenblatt, Y. Yaish, V. Sazonova, H. Üstünel, S. Braig, T. A. Arias, P. W. Brouwer, and P. L. McEuen, *Nano Lett.* **4**, 517 (2004).
- ³²A. Javey, J. Guo, M. Paulsson, Q. Wang, D. Mann, M. Lundstrom, and H. Dai, *Phys. Rev. Lett.* **92**, 106804 (2004).
- ³³T. Hertel and G. Moos, *Chem. Phys. Lett.* **320**, 359 (2000).
- ³⁴M. Y. Sfeir, T. Beetz, F. Wang, L. Huang, X. M. H. Huang, M. Huang, J. Hone, S. P. O'Brien, J. A. Misewich, T. F. Heinz, L. Wu, Y. Zhu, and L. E. Brus, *Science* **312**, 554 (2006).
- ³⁵F. Wang, M. Y. Sfeir, L. Huang, X. M. Henry Huang, Y. Wu, J. Kim, J. Hone, S. O'Brien, L. E. Brus, and T. F. Heinz, *Phys. Rev. Lett.* **96**, 167401 (2006).
- ³⁶Y. Wang, K. Kempa, B. Kimball, J. B. Carlson, G. Benham, W. Z. Li, T. Kempa, A. Rybczynski, and Z. F. Ren, *Appl. Phys. Lett.* **85**, 2607 (2004).
- ³⁷J. Rybczynski, K. Kempa, Y. Wang, Z. F. Ren, J. B. Carlson, B. R. Kimball, and G. Benham, *Appl. Phys. Lett.* **88**, 203122 (2006).